General Matrix Inversion Technique for the Calibration of Electric Field Sensor Arrays on Aircraft Platforms

D. M. Mach

University of Alabama in Huntsville, Huntsville, AL 35899, U.S.A.

and W. J. Koshak

NASA/Marshall Space Flight Center, Huntsville, AL 35812, U.S.A.

ABSTRACT: We have developed a matrix calibration procedure that uniquely relates the electric fields measured at the aircraft with the external vector electric field and net aircraft charge. Our calibration method is being used with all of our aircraft/electric field sensing combinations and can be generalized to any reasonable combination of electric field measurements and aircraft. We determine a calibration matrix that represents the individual instrument responses to the external electric field. The aircraft geometry and configuration of field mills (FMs) uniquely define the matrix. The matrix can then be inverted to determine the external electric field and net aircraft charge from the FM outputs. A distinct advantage of the method is that if one or more FMs need to be eliminated or de-emphasized (for example, due to a malfunction), it is a simple matter to reinvert the matrix without the malfunctioning FMs. To demonstrate our calibration technique, we present data from several of our aircraft programs (ER-2, DC-8, Altus, Citation).

1. Introduction

Measurements of electric fields within clouds have been made by aircraft for many years [*e.g., Gunn et al.,* 1946*; Blakeslee et al.,* 1989*; Winn,* 1993]. Retrieving electric field components from the raw aircraft FM data is perhaps the most difficult aspect of the measurement process [*e.g., Jones,* 1990*; Koshak et al.,* 1994; *Koshak,* 2006a; *Koshak et al.,* 2006b]. The electric field as measured by an instrument on the aircraft includes linear components from the external electric field (e_X, e_Y, e_Z), charge on the aircraft (e_Q), mill DC offset, and various other processes, including measurement errors and non-linear terms (γ). Typically we use electric field mills (i.e., mills) [*Bateman et al.,* 2006] as our electric field measuring instruments on aircraft. The equation relating the output of the i^{th} mill (a_i) to the external electric field components can be represented by:

$$a_i = M_{iX} e_X + M_{iY} e_Y + M_{iZ} e_Z + M_{iQ} e_Q + M_{iD} + \gamma \ , \qquad \textbf{(1)}$$

where the various M coefficients are the responses of the mills to the external field and charge on the aircraft, M_{iD} is the DC offset of the i^{th} mill, and we have neglected mill measurement errors.

For most techniques [e.g., *Koshak et al.,* 1994; *Koshak,* 2006a; *Koshak et al.,* 2006b], including ours, we neglect the non-linear terms so that the system can be solved with a linear algebraic approach. We also will neglect measurement errors in this analysis. That is, neglecting γ results in a linear set of equations between the mill outputs and the external electric fields. If you expand (1) in time and for all mills on an aircraft, the resultant system of equations are:

$$
\begin{aligned}
a_1(t) &= M_{1X}e_X(t) + M_{1Y}e_Y(t) + M_{1Z}e_Z(t) + M_{1Q}e_Q(t) + M_{1D} \\
a_2(t) &= M_{2X}e_X(t) + M_{2Y}e_Y(t) + M_{2Z}e_Z(t) + M_{2Q}e_Q(t) + M_{2D} \\
&\vdots \qquad\qquad\qquad\qquad \vdots \\
a_m(t) &= M_{mX}e_X(t) + M_{mY}e_Y(t) + M_{mZ}e_Z(t) + M_{mQ}e_Q(t) + M_{mD} \ ,
\end{aligned}
\tag{2}
$$

where m is the number of mills on the aircraft.

The mill DC offset are due to a number of factors that can change from day to day and even during a flight, but are usually small and are not significant during storm overflights. However, the offsets can be significant when compared to fair weather fields (when we usually do our calibrations). The reason why we explicitly call out this term will become clear later in the description of our calibration procedure.

The set of equations in (2) can be represented by a matrix equation:

$$
\mathbf{a}(t) = \mathbf{M}\mathbf{e}(t) \ , \tag{3}
$$

where $\mathbf{a}(t)$ is the vector of mill outputs as a function of time:

$$
\mathbf{a}(t) = \begin{bmatrix} a_1(t) \\ a_2(t) \\ a_3(t) \\ \vdots \\ a_m(t) \end{bmatrix} , \tag{4}
$$

$\mathbf{e}(t)$ is the vector external electric field (including the charge on the aircraft) as a function of time:

$$
\mathbf{e}(t) = \begin{bmatrix} e_X(t) \\ e_Y(t) \\ e_Z(t) \\ e_Q(t) \\ 1 \end{bmatrix} , \tag{5}
$$

and $\mathbf{M}$ is the m x 5 calibration matrix:

$$\mathbf{M} = \begin{bmatrix} M_{1X} & M_{1Y} & M_{1Z} & M_{1Q} & M_{1D} \\ M_{2X} & M_{2Y} & M_{2Z} & M_{2Q} & M_{2D} \\ \vdots & \vdots & \vdots & \vdots & \vdots \\ M_{mX} & M_{mY} & M_{mZ} & M_{mQ} & M_{mD} \end{bmatrix}. \tag{6}$$

Note the last row in $\mathbf{e}(t)$ and the last column in $\mathbf{M}$. As discussed above, these factors are introduced to account for (and thereby eliminate the effect of) mill offsets in our calibration procedure. How these terms affect the calibration will be discussed in later sections. For clarity, note that we use capital letters for matrices and small letters for vectors throughout our description of our method.

As given in (3), the matrix $\mathbf{M}$ relates the mill outputs to the external electric field and charge on the aircraft. The matrix $\mathbf{M}$ is constant and unique for each aircraft and mill distribution. Given $\mathbf{M}$, one can directly determine the outputs of the mills on the aircraft based on the external electric field vector. However, what we have are the mill outputs, $\mathbf{a}(t)$, and what we want is the external electric field vector, $\mathbf{e}(t)$. Pre-multiplying (3) by the transpose matrix $\mathbf{M}^T$ and pre-multiplying again by the square matrix $\left(\mathbf{M}^T\mathbf{M}\right)^{-1}$ gives:

$$\begin{aligned} \left[(\mathbf{M}^T\mathbf{M})^{-1}\mathbf{M}^T\right]\mathbf{M}\mathbf{e}(t) &= \left[(\mathbf{M}^T\mathbf{M})^{-1}\mathbf{M}^T\right]\mathbf{a}(t) \\ \mathbf{I}\mathbf{e}(t) &= (\mathbf{M}^T\mathbf{M})^{-1}\mathbf{M}^T\mathbf{a}(t) \\ \mathbf{e}(t) &= \mathbf{C}\mathbf{a}(t)\ , \end{aligned} \tag{7}$$

where $\mathbf{I}$ is the identity matrix and $\mathbf{C} \equiv (\mathbf{M}^T\mathbf{M})^{-1}\mathbf{M}^T$ which is the Moore Penrose (MP) 'pseudoinverse' [*Penrose*, 1955] of $\mathbf{M}$. In Matlab®, the function call is $\mathbf{C} = pinv(\mathbf{M})$. All of our mathematical analysis was done using the Matlab® software package. For simplicity, we will use the notation one would use in the Matlab® command line whenever possible. However,

we will expand the very compact notation when needed to explain what mathematical manipulations are actually used by the software package.

The elements of $\mathbf{C}$ are similar to the elements of $\mathbf{M}$ in that they relate the mill outputs to the external electric field (with net aircraft charge). For example, $e_X(t)$ is related to the mill outputs by:

$$e_X(t) = C_{X1}a_1(t) + C_{X2}a_2(t) + C_{X3}a_3(t) + \cdots + C_{Xm}a_m(t) \ , \qquad \textbf{(8)}$$

where the various C's are the first row of the $\mathbf{C}$ matrix. The electric field solution in (7) is termed the least-squares solution since it is the minimum of the scalar $s(\mathbf{e}) = (\mathbf{a} - \mathbf{Me})^2$.

2. Calibration Procedure

We use several techniques to minimize the errors in the retrieved elements of $\mathbf{M}$, which we will describe here. We have used this procedure to calibrate the FM systems installed on various aircraft (e.g., ER-2, DC-8, Citation, and Altus). The general steps are illustrated in Figure 1. Our overall strategy is to compute an initial estimate of $\mathbf{M}$ given by $\mathbf{M}_o$, and then perform $j = 1,...,P$ subsequent iterations to obtain refined estimates of $\mathbf{M}$ (i. e., $\mathbf{M}_1, \mathbf{M}_2, ..., \mathbf{M}_P$), where $\mathbf{M}_P$ is our best estimate of $\mathbf{M}$.

To compute $\mathbf{M}_o$, we first mount the mills on the aircraft in appropriate locations (step 1 in Figure 1). The next step is to fly the aircraft through a "known" electric field (such as the fair weather atmospheric field) while putting the aircraft through a series of roll and pitch calibration maneuvers and recording mill outputs (step 2). The next step is to make an ideal estimate of the external electric field in the aircraft frame-of-reference (step 3 in Figure 1) based on the model field profile (fair weather or other know field conditions) and the aircraft roll and pitch

maneuvers. The ideal electric field in the aircraft frame is combined with the mill outputs to compute $\mathbf{M}_o$ (step 4 in Figure 1).

Next, $\mathbf{M}_o$ is corrected for any known matrix symmetries (step 5). The corrected $\mathbf{M}_o$ matrix is inverted and combined with the mill outputs to create an estimate of the true electric field (step 6). This estimate of the electric field is corrected for any known problems (step 7 in Figure 1). It is then used to create the next iterate $\mathbf{M}_1$ matrix (step 4 of Figure 1). The $j = j+1$ iteration loop in Figure 1 is repeated until $\mathbf{M}_j$ converges. The $\mathbf{M}_j$ matrix usually stabilizes after about five iterations, but the general convergence conditions have not been proven or guaranteed. We then make an absolute calibration of the $\mathbf{M}_p$ matrix to create our best estimate of the true $\mathbf{M}$ matrix. The details of each of these steps will be covered in the following sections.

2.1. Mill Locations (Step 1)

Obviously, the very first step in the calibration procedure is to choose good locations for the field mills (step 1 in Figure 1). A proper placement of mills on an aircraft leads to an accurate calibration, while poor placement leads to excessive calibration errors which can totally mask the true $\mathbf{M}$ matrix. In our method, each mill should measure at least one component of electric field, and each component of the field should be dominate in at least one mill. Ideally, the mills should be distributed so that no two mills have similar sets and polarities of dominate field components and, if possible, both polarities of each component should be represented. That way, each mill will contribute to the measurement of the external fields.

An example mill placement for an ideal aircraft is shown in Figure 2 (top example 'A'). Note that each mill has at least one dominate component of the external electric field (and net aircraft charge) and each component is dominate in at least one mill. Further note that different

polarities are present for many of the field components. The polarity changes make it easier to remove the effects of aircraft charge. This placement of mills would make the calibration process easier. An example of a poor mill placement is also shown in Figure 2 (bottom example 'B'). Although the mills have dominate components in e_X, e_Y and e_Z, they all have approximately the same dominance in e_Y and e_Z. Since all mills would then react similarly to e_Y and e_Z, it would be very difficult to determine the e_Y and e_Z fields from this mill placement.

2.2. Calibration Data (Step 2)

Although any set of measurements of external electric fields can be used for calibration, it is best to pick data when the field values can be easily estimated. For example in our calibrations, we usually use field data during periods when the aircraft is performing roll and pitch maneuvers in fair weather conditions. Under such conditions, the external vector electric field is predominantly vertical with a profile that can be estimated [*e.g., Gish*, 1944]. The roll and pitch maneuvers map the assumed vertical fair weather field into the aircraft frame e_X, e_Y and e_Z components. An example of a set of calibration maneuvers for one of our aircraft is shown in Figure 3. Figure 4 shows the mill outputs during the roll and pitch maneuvers in Figure 3.

Our calibration technique works best when the various field components in the aircraft frame of reference are distinctly different and varying. Such times are when the aircraft is actually performing the pitch and roll maneuvers. Therefore, to maximize the convergence of our technique, we attempt to use field values only when they are changing due to the pitch and roll maneuvers. Attempting to fit the ideal fields to the mill outputs during times when the ideal fields are constant will often result in the solution fitting the field changes that are not traceable to

the roll and pitch maneuvers (such as fields due to charge pockets or thermals). By focusing on the roll and pitch maneuvers, we force the least-squares solution to model those waveforms and not waveforms from other sources. For example, Figure 5 shows the ideal fields during the calibration maneuvers from Figures 3 and 4. The variations in the fields should be readily identifiable. A poor choice of calibration data is shown in Figure 6. During this time period, the Citation aircraft was not making any significant calibration maneuvers. Note the various features in the mill outputs that are not reflected in the ideal fields. Using this time period to calibrate our aircraft mill configuration would produce a poor estimate of **M** very different from the one based on the data in Figure 3.

2.3. First Estimate of the External Electric Field (Step 3)

Given fair weather fields (derived from *Gish* [1944]), and the aircraft roll, pitch, and altitude information, we can derive first guess or ideal external electric fields in the aircraft frame of reference. These are shown in Figure 5 (plots g_X, g_Y, and g_Z) for the calibration example used in Figures 3 and 4. To determine the g_Q coefficient, we need to have charge induced on the aircraft frame. Often this is done with a high voltage stinger probe [e.g., *Vonnegut et al.*, 1961], however, charges induced on the aircraft due to the maneuvers or power changes can be used if a stinger is not available. In addition, we have found that the fields at the mills are often dominated by the charge on the aircraft even while flying in fair weather conditions. Since the other components are small and are often alternating polarities in different mills (some mills have positive components, some have negative), the sum of the mill outputs is often almost exclusively due to the charge on the aircraft. Therefore, we can use the average mill value (summed over all mills) as a first guess to the fields at the mills due to charge on the aircraft (g_Q). Note that there

is no "absolute" value of g_Q. All that is needed is a relative value so that the effects of charge on the aircraft can be separated from the other components. The first guess as to the field due to charge on the aircraft are also shown in Figure 5 (plot g_Q).

2.4. The First Estimate of M (Step 4 with $j = 0$)

To produce the first guess of the **M** matrix ($\mathbf{M}_o$), we gather the mill outputs as a function of time into an m x n matrix **A**:

$$\mathbf{A} = \left[\mathbf{a}(t_1)\ \mathbf{a}(t_2)\ \mathbf{a}(t_3)\ \cdots\ \mathbf{a}(t_n)\right] , \tag{9}$$

where each $\mathbf{a}(t_i)$ is the column vector of m mill measurements at time t_i and n is the number of observation times used from the calibration period. We then collect the first guess of the external fields (including aircraft charge) into a 5 x n matrix **G**:

$$\mathbf{G} = \left[\mathbf{g}(t_1)\ \mathbf{g}(t_2)\ \mathbf{g}(t_3)\ \cdots\ \mathbf{g}(t_n)\right] . \tag{10}$$

Each column vector $\mathbf{g}(t)$ is a first guess of the electric field in (5) at a particular time, and is based on the field profile and aircraft roll and pitch maneuvers, and n is as described for (9). It can also be called the "ideal" fields as **G** is the field that would be present if the field profile was correct and there were no other contributions to the electric field (such as charge pockets). We then obtain $\mathbf{M}_o$ by Matlab® right matrix division:

$$\mathbf{M}_o = \mathbf{A}/\mathbf{G} , \tag{11}$$

which is a short-hand representation of the least squares solution [*Anderson et al.*, 1999] for finding $\mathbf{M}_o$. The definition of this matrix division is provided in the Appendix.

We have found that the most common source of non-field components are DC offsets in the mill outputs. To prevent the mill DC offsets from distorting our calibration, note that the fifth row of $\mathbf{G}$ contains all 1s, and the contributions to the mill outputs from the offsets (which are constant over the time of the calibration) are hence contained in the fifth column of $\mathbf{M}_o$. DC offsets cannot easily distort the minimization of the other components because of this arrangement of constant terms. This approach is used for all subsequent iterations to prevent the mill offsets from biasing solution $\mathbf{M}_P$.

2.5. The j^{th} Estimate of E (Steps 5 and 6)

Once we have the $\mathbf{M}_o$ matrix (including the offset terms), or more generally any iterate $\mathbf{M}_j$, we correct it for any know aircraft symmetries (step 5). For example, a mill mounted along the centerline of an aircraft should not have significant e_Y components. We call the corrected matrix $\mathbf{M}_j^*$. In step 6, we take the MP pseudoinverse to obtain:

$$\mathbf{C}_j = pinv(\mathbf{M}_j^*) \;\; ; \quad j = 0,1,\ldots,P\,. \tag{12}$$

Invoking (7), we estimate the true external electric fields with:

$$\mathbf{F}_j = \mathbf{C}_j\mathbf{A}\;, \tag{13}$$

where $\mathbf{F}_j$ is the 5 x n matrix of the j^{th} estimate of the true external electric fields:

$$\mathbf{F}_j = \begin{bmatrix} f_X(t_1) & f_X(t_2) & f_X(t_3) & \cdots & f_X(t_n) \\ f_Y(t_1) & f_Y(t_2) & f_Y(t_3) & \cdots & f_Y(t_n) \\ f_Z(t_1) & f_Z(t_2) & f_Z(t_3) & \cdots & f_Z(t_n) \\ f_Q(t_1) & f_Q(t_2) & f_Q(t_3) & \cdots & f_Q(t_n) \\ f_D(t_1) & f_D(t_2) & f_D(t_3) & \cdots & f_D(t_n) \end{bmatrix}_j . \tag{14}$$

The first four rows of $\mathbf{F}_j$ are the various field components (including aircraft charge) while the last row approximates a row of 1s (i.e., as $\mathbf{M}_j$ approaches $\mathbf{M}$, the last row of $\mathbf{F}_j$ approaches a row of 1s).

Although the ideal electric field, $\mathbf{G}$, is a good first guess, the estimated electric field, $\mathbf{F}_j$, often have temporal and spatial variations that are not found in the ideal fields. For example, Figure 7 compares $\mathbf{G}$ (ideal fields, gray waveform) with $\mathbf{F}_o$ (estimated fields, black waveform) during a calibration run. Note that the fields are much more variable in the "true" case. Many of the "bumps" in $\mathbf{F}_o$ correspond to roll and pitch maneuvers (as indicated in the $\mathbf{G}$ waveform), however, there are a number of excursions in $\mathbf{F}_o$ that are not caused by the roll and pitch maneuvers. Attempting to force the $\mathbf{M}_j$ matrix to fit $\mathbf{G}$ when $\mathbf{F}_j$ is more like the true fields can introduce significant errors in the matrix determination process.

2.6. Correction of $\mathbf{F}_j$ (Step 7)

The next step is to correct the components of $\mathbf{F}_j$. To do so, we must introduce the true electric fields at times t_1 to t_n (the actual e_X, e_Y, e_Z, and e_Q fields at the measurement times):

$$\mathbf{E} = \begin{bmatrix} e_X(t_1) & e_X(t_2) & e_X(t_3) & \cdots & e_X(t_n) \\ e_Y(t_1) & e_Y(t_2) & e_Y(t_3) & \cdots & e_Y(t_n) \\ e_Z(t_1) & e_Z(t_2) & e_Z(t_3) & \cdots & e_Z(t_n) \\ e_Q(t_1) & e_Q(t_2) & e_Q(t_3) & \cdots & e_Q(t_n) \\ 1 & 1 & 1 & \cdots & 1 \end{bmatrix}, \quad \textbf{(15)}$$

which is a 5 x n matrix. Combining (3), (9), and (13) gives:

$$\begin{aligned}\mathbf{F}_j = \mathbf{C}_j\mathbf{A} &= \mathbf{C}_j\left[\mathbf{a}(t_1)\ \mathbf{a}(t_2)\ \mathbf{a}(t_3)\ \cdots\ \mathbf{a}(t_n)\right] \\ &= \mathbf{C}_j\left[\mathbf{Me}(t_1)\ \mathbf{Me}(t_2)\ \mathbf{Me}(t_3)\ \cdots\ \mathbf{Me}(t_n)\right] \\ &= \mathbf{C}_j\mathbf{ME} \\ \therefore\ \mathbf{F}_j &= \mathbf{H}_j\mathbf{E}\ ,\end{aligned} \tag{16}$$

where the 5 x 5 matrix $\mathbf{H}_j$ is a constant defined by:

$$\mathbf{H}_j \equiv \mathbf{C}_j\mathbf{M} = \begin{bmatrix} H_{XX} & H_{XY} & H_{XZ} & H_{XQ} & H_{XD} \\ H_{YX} & H_{YY} & H_{YZ} & H_{YQ} & H_{YD} \\ H_{ZX} & H_{ZY} & H_{ZZ} & H_{ZQ} & H_{ZD} \\ H_{QX} & H_{QY} & H_{QZ} & H_{QQ} & H_{QD} \\ H_{DX} & H_{DY} & H_{DZ} & H_{DQ} & H_{DD} \end{bmatrix}_j . \tag{17}$$

From the result in (16), one can write any estimated field component, for example, the X-component, as:

$$f_X(t_i) = H_{XX}e_X(t_i) + H_{XY}e_Y(t_i) + H_{XZ}e_Z(t_i) + H_{XQ}e_Q(t_i) + H_{XD}\ , \tag{18}$$

where it is understood that this is associated with the jth iteration; i.e., we drop the j index on the f and H scalars for brevity.

Note that as $\mathbf{M}_j$ approaches $\mathbf{M}$, $\mathbf{C}_j$ in (12) approaches $(\mathbf{M}^T\mathbf{M})^{-1}\mathbf{M}^T$, and hence $\mathbf{H}_j = \mathbf{C}_j\mathbf{M} = (\mathbf{M}^T\mathbf{M})^{-1}\mathbf{M}^T\mathbf{M} = \mathbf{I}$. In other words, if $\mathbf{M}_j$ approaches $\mathbf{M}$, $f_X(t_i)$ approaches $e_X(t_i)$ because the diagonal elements of $\mathbf{H}_j$ approach unity while the off diagonal elements of $\mathbf{H}_j$ approach zero. The meaning of (18) is that each component of $\mathbf{F}_j$ is dominated by the same component of $\mathbf{E}$ (i.e., the diagonal elements of $\mathbf{H}_j$), with smaller contributions from the other components of $\mathbf{E}$ (i.e., the non-diagonal elements of $\mathbf{H}_j$). By looking for features in the various $\mathbf{F}_j$ waveforms that are due to the various $\mathbf{E}$ components we expect from the calibration

maneuvers, we can estimate the contamination of the various components of $\mathbf{F}_j$, (the non-diagonal elements of $\mathbf{H}_j$) and subtract them to produce an $\mathbf{F}_j$ closer to $\mathbf{E}$.

An example of a $\mathbf{F}_o$ (based on the first guess $\mathbf{M}_o$ and the actual mill outputs) along with $\mathbf{G}$ fields is shown in Figure 8. We know that the details of $\mathbf{E}$ will be different than $\mathbf{G}$, but the major transitions will be due to the roll and pitch maneuvers, which will be very similar in both $\mathbf{E}$ and $\mathbf{G}$. In this example, f_X (with $j = 0$, i.e., the fields based on the first guess $\mathbf{M}_o$) has e_Y and/or e_Z contamination while f_Y and f_Q each have e_X contamination. We can identify these cross-contaminations because we are monitoring the aircraft electric fields during times when we approximately know what the fields should be doing (i.e., the $\mathbf{G}$ fields). For example in Figure 8, during the period 16:14 to 16:15, the aircraft is making pitch maneuvers. We know that during that time, the e_X and e_Z fields should be varying while the e_Y and e_Q fields should be more or less constant. Therefore, the "bumps" in the f_Q and f_Y fields during that time that resemble the e_X excursions are likely due to contaminations of those components by e_X. By comparing the amplitude of the "bumps" in the f_Y (due to e_X contamination), we can estimate the amount of contamination and subtract a portion of f_X from f_Y to produce the improvement f_Y' (as show in Figure 9):

$$f_Y' = f_Y - \alpha f_x \ , \tag{19}$$

where α is an empirically determined factor that is set to best eliminate the cross-contamination. As shown in Figure 9, we perform the same operations on the f_X, f_Z, and f_Q components to obtain the corrected $\mathbf{F}_j$, which we write as $\mathbf{F}_j'$.

One of the reasons this step is done by hand is it is difficult to identify the "bumps" associated with the calibration maneuvers under "real world" conditions (as seen in Figures 8 and 9). Many of the "bumps" (such as the ones in f_Z and f_Q around 16:17) are not readily identifiable as due to calibration maneuvers. We have found that these bumps not due to calibration rolls or pitches make automatic processing of the calibration data impossible.

2.7. Subsequent Estimates of M (step 4 with $j \geq 1$)

Next, note in Figure 1 that j is incremented. This means that the $\mathbf{F}'_j$ discussed above is now written as $\mathbf{F}'_{j-1}$. Hence, the next iterate (and all subsequent iterates) are written as:

$$\mathbf{M}_j = \mathbf{A}/\mathbf{F}'_{j-1}; \quad j = 1, \ldots, P \quad , \tag{20}$$

where $\mathbf{A}$ is again the mill outputs given in (9). The process is repeated until the j^{th} iterate $\mathbf{M}_j$ converges and the field outputs ($\mathbf{F}_j$) stabilize to reasonable waveforms (like those in Figure 9). The (relative) calibration matrix obtained is $\mathbf{M}_P$. Convergence here simply means that the last few iterates ($\mathbf{M}_{P-2}, \mathbf{M}_{P-1}, \mathbf{M}_P$) differ by a sufficiently small amount. For typical combinations of FM, data, and aircraft, this process usually takes about five iterations, with the majority of the iterations used to fully identify the various components in the true electric field (i.e., which 'bumps' in the waveforms are caused by which components of the true electric field).

2.8. Absolute Calibration (Step 8)

The steps in the previous sections only provide a relative calibration, that is, the components in $\mathbf{F}_P$ are correctly proportioned to the components in $\mathbf{E}$. However, each component may differ (in a unique way) by a multiplicative constant from their true magnitude. Essentially,

we have created a $\mathbf{F}$ with the correct waveshapes, but not the correct amplitudes. We can determine the relative multiplicative constants between the various components (e.g., f_X, f_Y, & f_Z) by checking the relative responses of the various components to the roll and pitch maneuvers. However, even after this step, we need one more constant to create a final calibration matrix.

To determine the final multiplicative constant, we need to compare our fields calculated with the final $\mathbf{M}_P$ matrix to a known electric field. This is typically accomplished by flying the aircraft near a calibrated ground based mill and comparing the relative amplitudes of the fields at the ground and at the aircraft. The ratio of the two fields produces the factors needed in the final absolute calibration of the $\mathbf{M}$ matrix. Figure 10 shows an example ground-based mill overflight for one of our aircraft platforms.

3. Results

We have used this calibration method to create $\mathbf{M}_P$ matrices for four different aircrafts. Figure 11 show the electric fields based on the final calibration of the FMs on the NASA ER-2 [*Hood et al.*, 2006]. Figure 12 shows the electric field vector based on the final calibration of the mills on the North Dakota Citation [*Dye et al.*, 2004]. Figure 13 shows the vector electric field components based on the final $\mathbf{M}_P$ matrix for an overflight of a small storm with the NASA DC-8. Figure 14 shows the fields during an overpass of a thunderstorm with the Altus aircraft [*Mach et al.*, 2005] based on the final $\mathbf{M}_P$ matrix for that aircraft and FM combination. In each case, the aircraft flew over and slightly to the side of the electrified cloud.

For such overflights of typical storms (positive charge near the top of the storms), the e_X field component should first go negative as the aircraft approaches, pass through zero at the

closest approach to the storm, reach a positive peak, and then decay away to zero as the aircraft recedes from the storm. If the aircraft passes directly over the center of the charge, the e_Y field should be close to zero. However, if the aircraft passes to the side of the storm, the field trace should have somewhat of a Gaussian shape with the polarity depending on which side the aircraft passed. The e_Z field should also have a Gaussian shape with positive polarity. The shape of the e_Q component depends on so many different factors that it is difficult to characterize. Any lightning will be superimposed on these general shapes.

The wave shapes in Figures 11, 12, 13, and 14 follow these general trends, indicating that the calibrations based on our **M** matrix method are reasonable. Unfortunately, further verification of the calibrations requires knowledge of the electric fields that we simply do not have.

4. Mill Output Weighting

Once the final $\mathbf{M}_P$ matrix is calculated, the inversion process can be used to create a **C** matrix with user defined properties. For example, if a **C** matrix is formed using the following formula:

$$\mathbf{C} = pinv(\mathbf{W}\mathbf{M}_P)\mathbf{W} \ , \tag{21}$$

where **W** is a m x m diagonal weighting matrix. The diagonal elements of **W** (i.e., W_{ii}, $i = 1,...,m$) will determine how much the i^{th} mill is emphasized in the resultant **C** matrix. For example, given an aircraft instrumented with 6 mills, we can take mill #3 totally out of the **C** matrix by simply nullifying element W_{33}. With the remaining five mills equally weighted, **W** is written as:

$$\begin{bmatrix} 1 & 0 & 0 & 0 & 0 & 0 \\ 0 & 1 & 0 & 0 & 0 & 0 \\ 0 & 0 & 0 & 0 & 0 & 0 \\ 0 & 0 & 0 & 1 & 0 & 0 \\ 0 & 0 & 0 & 0 & 1 & 0 \\ 0 & 0 & 0 & 0 & 0 & 1 \end{bmatrix}, \tag{22}$$

where the element corresponding to the third row, third column is zero. As long as the original $\mathbf{M}_P$ was correct, the resultant $\mathbf{C}$ matrix will create valid fields, but have no contributions from mill #3. The diagonal elements of $\mathbf{W}$ need not take on binary values (shutting on or off mills), but can assume arbitrary values to emphasize or de-emphasize mills in any way pleased based on the specific quality of individual mill outputs. For example, to lower the influence of mill #3 by a factor of ten, the zero in W_{33} in (22) would be replaced by 0.1.

4.1. Example Use of W

Figure 15 shows the mill outputs during a time when one of the mills was malfunctioning (mill QL). Figure 16 shows the field values based on the $\mathbf{C}$ matrix with all mills (including the malfunctioning mill). Note the significant errors in the plots. All of the field components are essentially masked by the mill errors. If we produce a $\mathbf{W}$ matrix with element W_{22} equal to 0.1 and use (21) to compute $\mathbf{C}$, we get the data in Figure 17. Note that the influence of mill #2 is much less. If we produce a $\mathbf{W}$ matrix with element W_{22} equal to 0, we get the data in Figure 18. Note that the noise from mill #2 is totally eliminated.

Each $\mathbf{C}$ matrix was based on the same $\mathbf{M}_P$ matrix but with different $\mathbf{W}$ matrices. Figure 19 shows the expanded f_Q component for each of the three different cases (no weighting,

mill #2 reduced by a factor of 10, mill #2 totally removed). Note that the overall field component shape is the same in each case. The only difference is the influence of the noise from mill #2.

Reasons for reducing the influence of a mill, instead of simply eliminating it, include cases where the mill is critical for determining one component of the external electric field. For example, one of our aircraft had four mills mounted in a similar way to mills two through six in Figure 2. The aft mill was critical in the estimation of e_X, but due to the mounting location, its output was often very noisy. By setting its weighting function to 0.1, we were able to significantly reduce its influence on the e_Y, e_Z, and e_Q components (where it was not needed) while still using it to determine e_X (where it was critical).

4.2. Other Uses of M Matrix Method

If the real-time analysis program stores $\mathbf{M}_P$ and calculates $\mathbf{C}$ on-the-fly, mill health information can be used to modify which mills are used in the determination of the field values by manipulating the $\mathbf{W}$ matrix in (21). This would allow for real-time changes in the calculation of field values based on mill metadata. Individual mills could be turned off and on, or their influence simply reduced based on their health in real-time.

5. Conclusion

We have developed a method of determining the relationship between the external electric fields and the outputs of electric field meters for a generalized aircraft platform. As long as the FMs are not placed in a pathological fashion and there are more FMs than electric field components, the method converges after a few iterations. By determining the $\mathbf{M}$ matrix (the matrix that produces the FM outputs from the field values) instead of the $\mathbf{C}$ matrix (the matrix that produces the field values from the FM outputs), we can use the properties of the $\mathbf{M}$ matrix to

simplify the calibration process and also add the ability to emphasize or eliminate FM outputs on the fly.

Appendix

Solution Forms for the M Matrix

In this appendix, two standard solution forms for the **M** matrix are provided. One form was given in Koshak (2006a), and the other form is used in this paper an detailed here. It is then shown that the two forms are equivalent. This helps better establish the inter-relationship between Koshak (2006a) and the current writing.

In Koshak (2006a) the following solution form for **M** is provided. For $j = 1,...,n$ aircraft orientations of an aircraft having calibration matrix **M**, one can write the mill outputs $\mathbf{a}_j = \mathbf{a}(t_j)$ at time t_j due to ambient electric field $\mathbf{e}_j = \mathbf{e}(t_j)$ as

$$\mathbf{a}_j = \mathbf{M}\mathbf{e}_j \quad . \tag{A.1}$$

Next, each side of this equation is post-multiplied by the transpose $\mathbf{e}_j^T$, and then summed for all $j = 1,...,n$ orientations. This gives:

$$\sum_{j=1}^{n} \mathbf{a}_j \mathbf{e}_j^T = \sum_{j=1}^{n} \mathbf{M}\mathbf{e}_j \mathbf{e}_j^T = \mathbf{M} \sum_{j=1}^{n} \mathbf{e}_j \mathbf{e}_j^T$$

$$\Rightarrow \quad \mathbf{M} = \sum_{j=1}^{n} \mathbf{a}_j \mathbf{e}_j^T \left(\sum_{j=1}^{n} \mathbf{e}_j \mathbf{e}_j^T \right)^{-1} \quad . \tag{A.23}$$

This last expression in (A.2) is the first expression in (4) of Koshak (2006a), but here we omit mill errors and factors of $1/n$ for brevity.

In the main text of this paper, we have used a different notation. First, we defined the following two matrices:

$$\mathbf{A} = [\mathbf{a}_1 \ \mathbf{a}_2 \ \ldots \mathbf{a}_n], \quad \mathbf{E} = [\mathbf{e}_1 \ \mathbf{e}_2 \ \ldots \mathbf{e}_n] \tag{A.3}$$

which allow us to write all $j = 1,\ldots,n$ of the equations in (A.1) as

$$\mathbf{A} = \mathbf{ME} \ . \tag{A.4}$$

Postmultiplying by the transpose $\mathbf{E}^T$ and inverting gives

$$\mathbf{M} = \mathbf{A}\mathbf{E}^T(\mathbf{E}\mathbf{E}^T)^{-1} \ . \tag{A.5}$$

However, it can be shown by straightforward matrix multiplication that

$$\mathbf{A}\mathbf{E}^T = \sum_{j=1}^{n} \mathbf{a}_j \mathbf{e}_j^T \ , \quad \mathbf{E}\mathbf{E}^T = \sum_{j=1}^{n} \mathbf{e}_j \mathbf{e}_j^T \ . \tag{A.6}$$

Therefore, the solution for $\mathbf{M}$ in (A.2) given in Koshak (2006a) is identical to the solution in (A.5). In addition, note that the right matrix division defined by Matlab® and used in the main text (equation 11) is defined by (A.5), that is

$$\mathbf{M} = \mathbf{A}/\mathbf{E} \equiv \mathbf{A}\mathbf{E}^T(\mathbf{E}\mathbf{E}^T)^{-1} \ . \tag{A.7}$$

6. References

Anderson, E., Z. Bai, C. Bischof, S. Blackford, J. Demmel, J. Dongarra, J. Du Croz, A. Greenbaum, S. Hammarling, A. McKenney, and D. Sorensen, LAPACK User's Guide, Third Edition, SIAM, Philadelphia, 1999.

Blakeslee, R. J., H. J. Christian, and B. Vonnegut, Electrical measurements over thunderstorms, *J. Geophys. Res.*, **94,** 13135-13140, 1989.

Dye, J. E., S. A. Lewis, W. D. Hall, J. C. Willett, P. Willis, C. A. Grainger, D. Mach, M. Bateman, and H. J. Christian, Airborne observations of microphysics and electric fields in anvils of Florida thunderstorms, *14th International Conference on Clouds and Precipitation, II*, 1001-1004, 2004.

Gish, O. H., Evaluation and interpretation of the columnar resistance of the atmosphere, *Terr. Magn. Atmos Elec.*, **49,** 159-168, 1944.

Gunn, R., and J. P. Parker, The high-voltage characteristics of aircraft in flight, *Proc. IRE,* **34,** 241-247, 1946.

Hood, R. E., D. Cecil, F. J. LaFontaine, R. Blakeslee, D. Mach, G. Heymsfield, F. Marks, Jr., E. Zipser and M. Goodman, Tropical cyclone precipitation and electrical field information observed by high altitude aircraft instrumentation. *J. Atmos. Sci.*, **63**, 218-233, 2006.

Jones, J. J., Electric charge acquired by airplanes penetrating thunderstorms, *J. Geophys. Res.*, **95,** 16589-16600, 1990.

Koshak, W. J., J. C. Bailey, H. J. Christian, and D. M. Mach, Aircraft electric field measurements: Calibration and ambient field retrieval, *J. Geophys. Res.*, **99,** 22781-22792, 1994.

Koshak, W. J., Retrieving storm electric fields from aircraft field mill data. Part I: theory, *J. Atmos. Oceanic Technol.*, accepted for publication, 2006a.

Koshak, W. J., D. M. Mach, H. J. Christian, M. F. Stewart, M. Bateman, Retrieving storm electric fields from aircraft field mill data. Part II: applications, *J. Atmos. Oceanic Technol.*, accepted for publication, 2006b.

Mach, D. M., R. J. Blakeslee, J. C. Bailey, W. M. Farrell, R. A. Goldberg, M. D. Desch, and J. G. Houser, Lightning optical pulse statistics from storm overflights during the Altus Cumulus Electrification Study, *Atmos. Res.*, **76**, 386-401, 2005.

Penrose, R., A generalized inverse for matrices, *Proc. Cambridge Philos. Soc.* **51**, 406-413, 1955.

Winn, W. P., Aircraft measurement of electric field: Self-calibration, J. Geophys. Res., 98, 6351-6365, 1993.

Vonnegut, B., C. B. Moore, and F. J. Mallahan, Adjustable potential-gradient-measuring apparatus for airplane use, *J. Geophys. Res.*, **66,** 2393-2397, 1961.

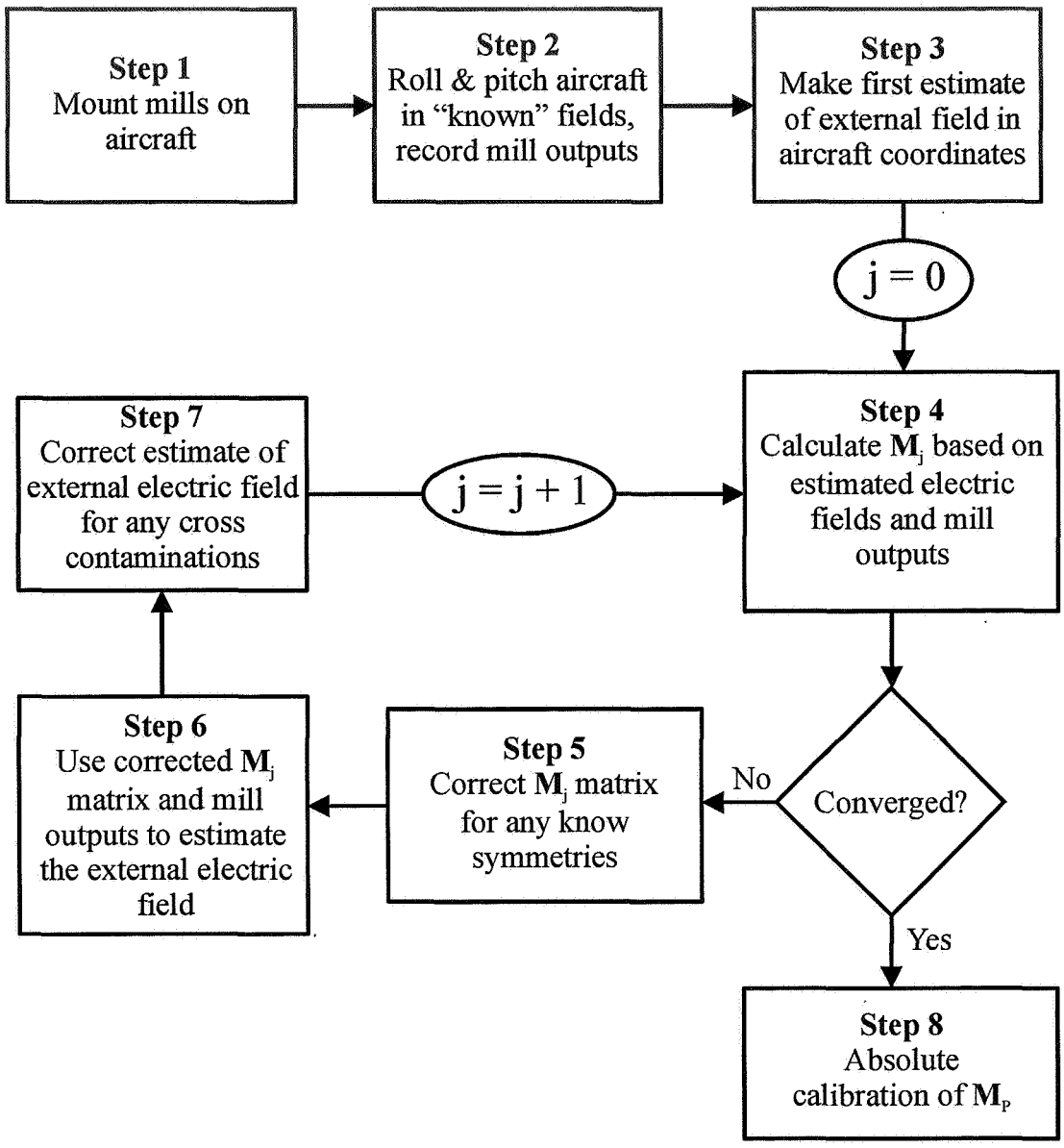

Figure 1. Steps used to estimate the **M** matrix. The process of refining the $\mathbf{M}_j$ matrix usually takes about five iterations (j = 0, 1, ..., 4) to settle to the point where further changes in the $\mathbf{M}_j$ matrix produce no discernable changes in the final electric field values. We do not correct the $\mathbf{M}_j$ matrix for any know symmetries on the aircraft the final time because the aircraft is not exactly symmetric. The best estimate is called $\mathbf{M}_P$ in the text. The final absolute calibration creates our best estimate of **M**.

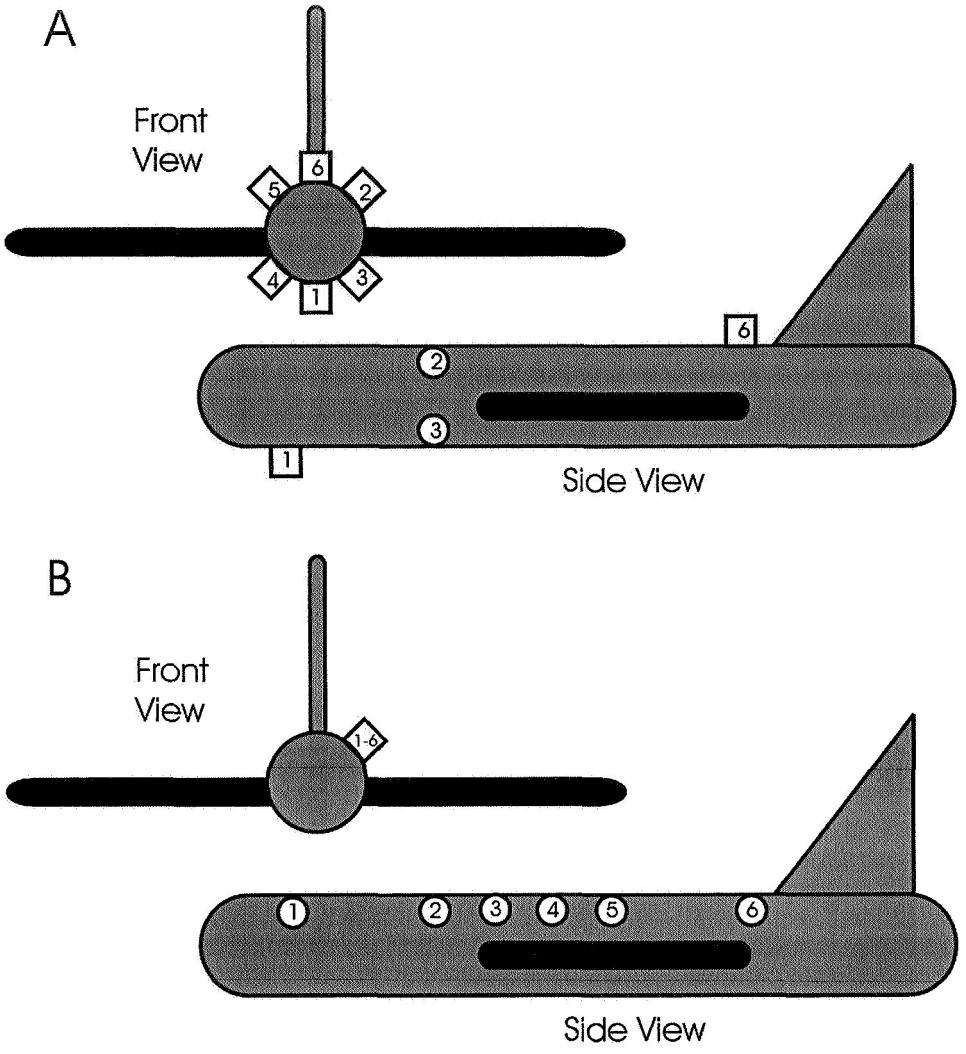

Figure 2. Example placements of mills on an ideal aircraft. Version "A" shows a "good" placement of mills. Mill #1 output is dominated by e_X and $-e_Z$. Mill #2 output is dominated by e_Y and e_Z. Mill #3 output is dominated by e_Y and $-e_Z$. Mill #4 output is dominated by $-e_Y$ and $-e_Z$. Mill #5 output is dominated by $-e_Y$ and e_Z. Mill #6 is dominated by $-e_X$ and e_Z. All mills have a strong e_Q component. Note that the mills have different dominate components of **E**. This configuration should converge using our calibration method. Version "B" shows a "poor" placement of mills. In this version all mills have similar values of e_Y and e_Z, making convergence of our calibration method difficult if not impossible.

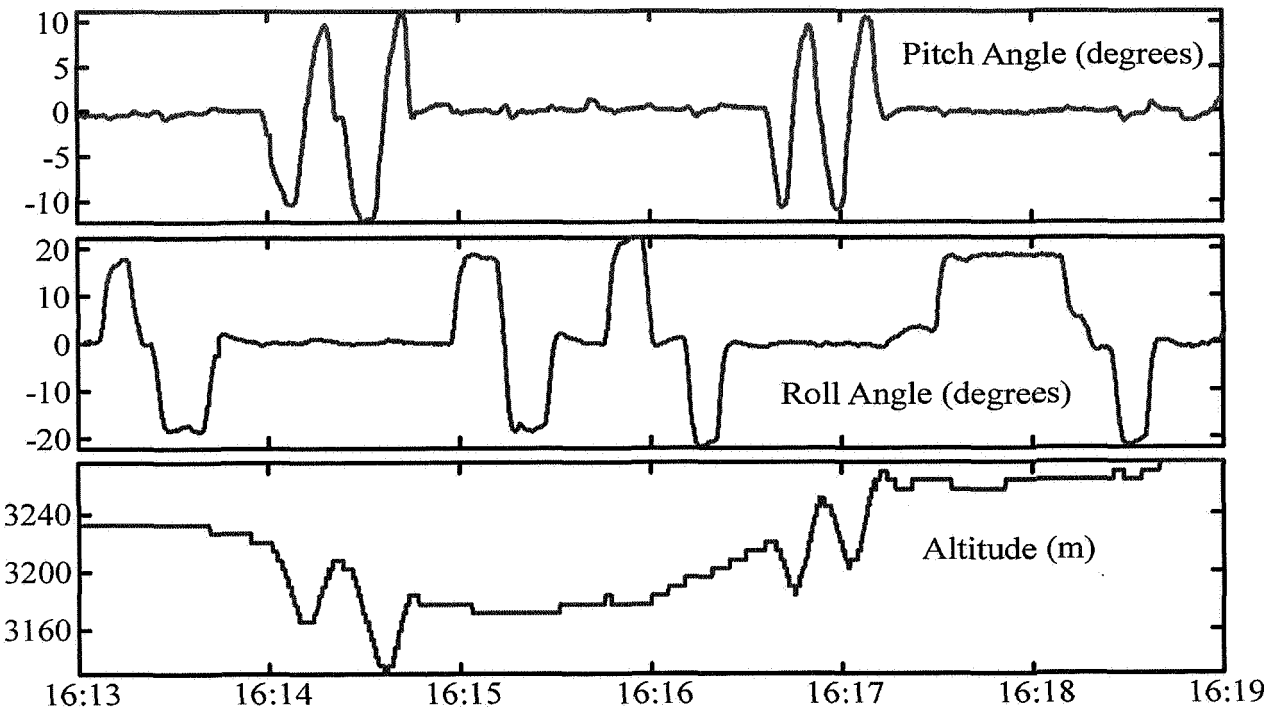

Figure 3. Example roll/pitch maneuver set obtained during the Altus aircraft calibration flight. The roll and pitch angles are in degrees while the altitude is in meters. The amplitude is in V/m and the time is in hours: minutes on July 11, 2002.

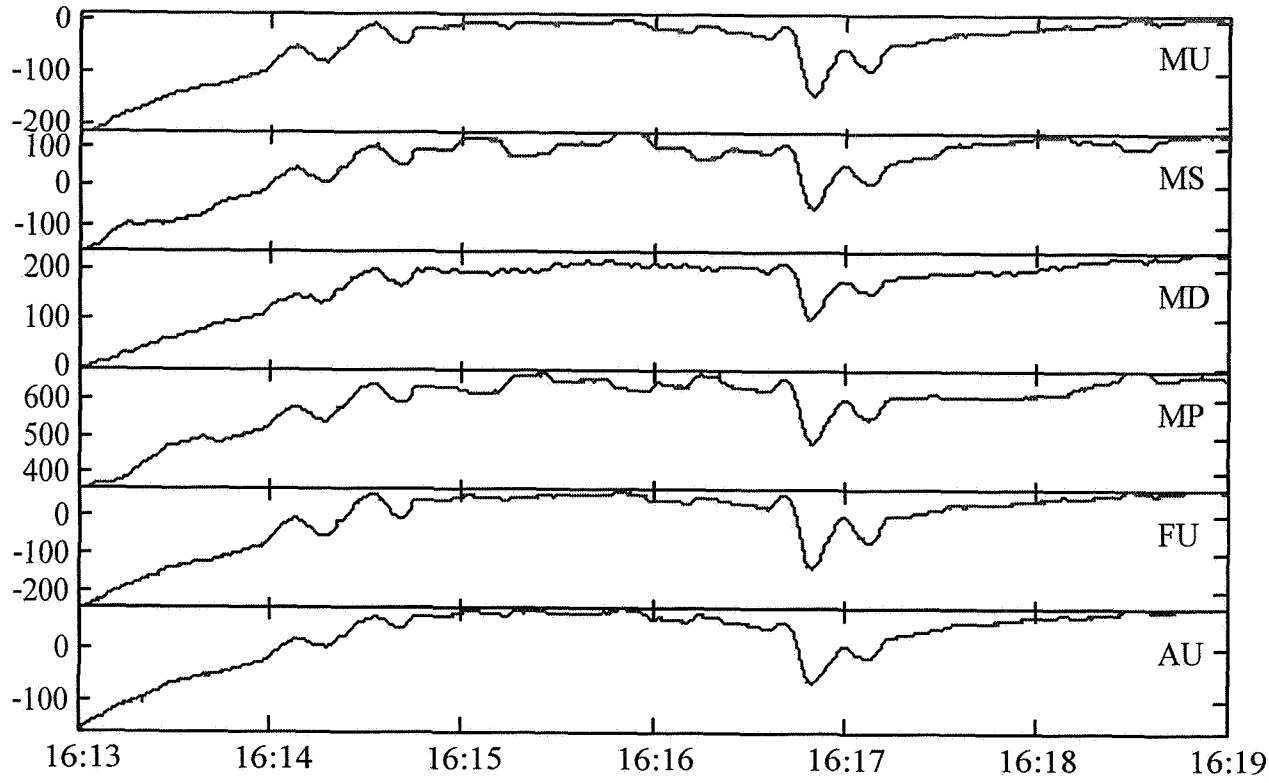

Figure 4. Electric field mill outputs during the roll/pitch maneuvers in Figure 3. There were six mills on the Altus aircraft designated 'Mid-Up' (MU), 'Mid-Starboard' (MS), 'Mid-Down' (MD), 'Mid-Port' (MP), 'Front-Up' (FU), and 'Aft-Up' (AU). The amplitude is in Volts per meter (V/m) and the time is in hours: minutes on July 11, 2002.

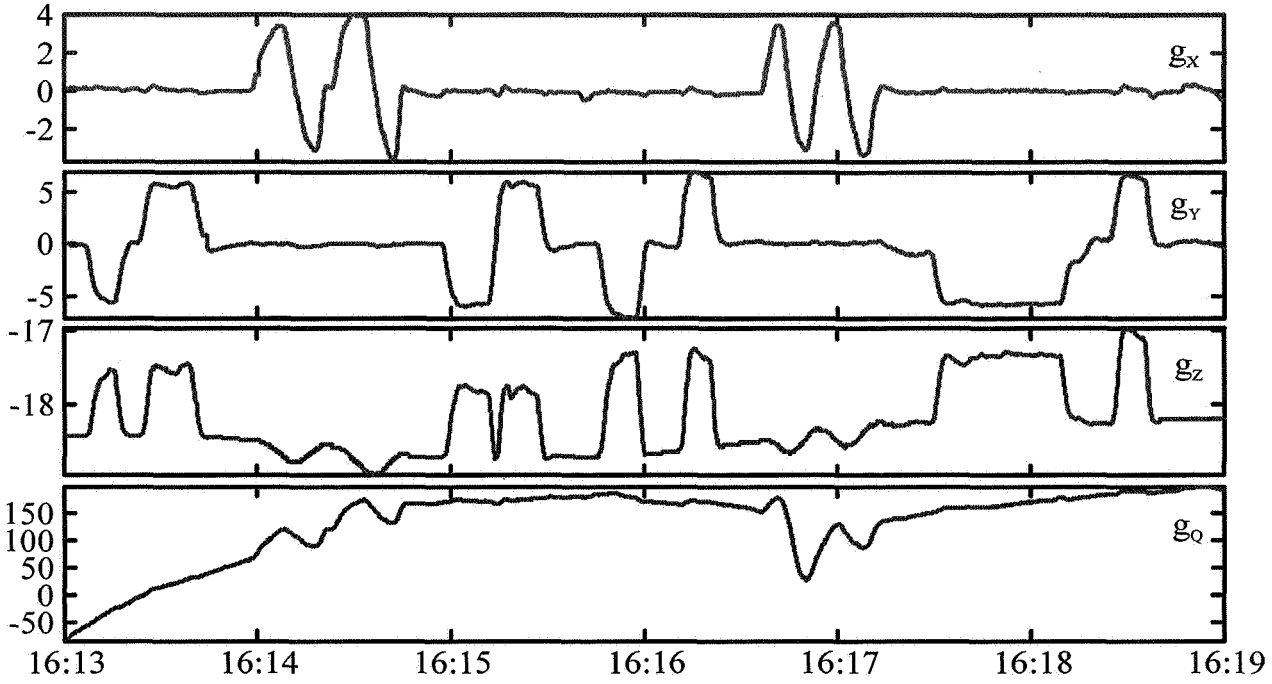

Figure 5. Ideal fields $(g_X(t), g_Y(t), g_Z(t), g_Q(t))$ in the aircraft frame of reference during the roll/pitch maneuvers from Figure 3. The $g_Q(t)$ component is estimated using the mean values of the 6 mill outputs. The amplitude is in V/m and the time is in hours: minutes on July 11, 2002.

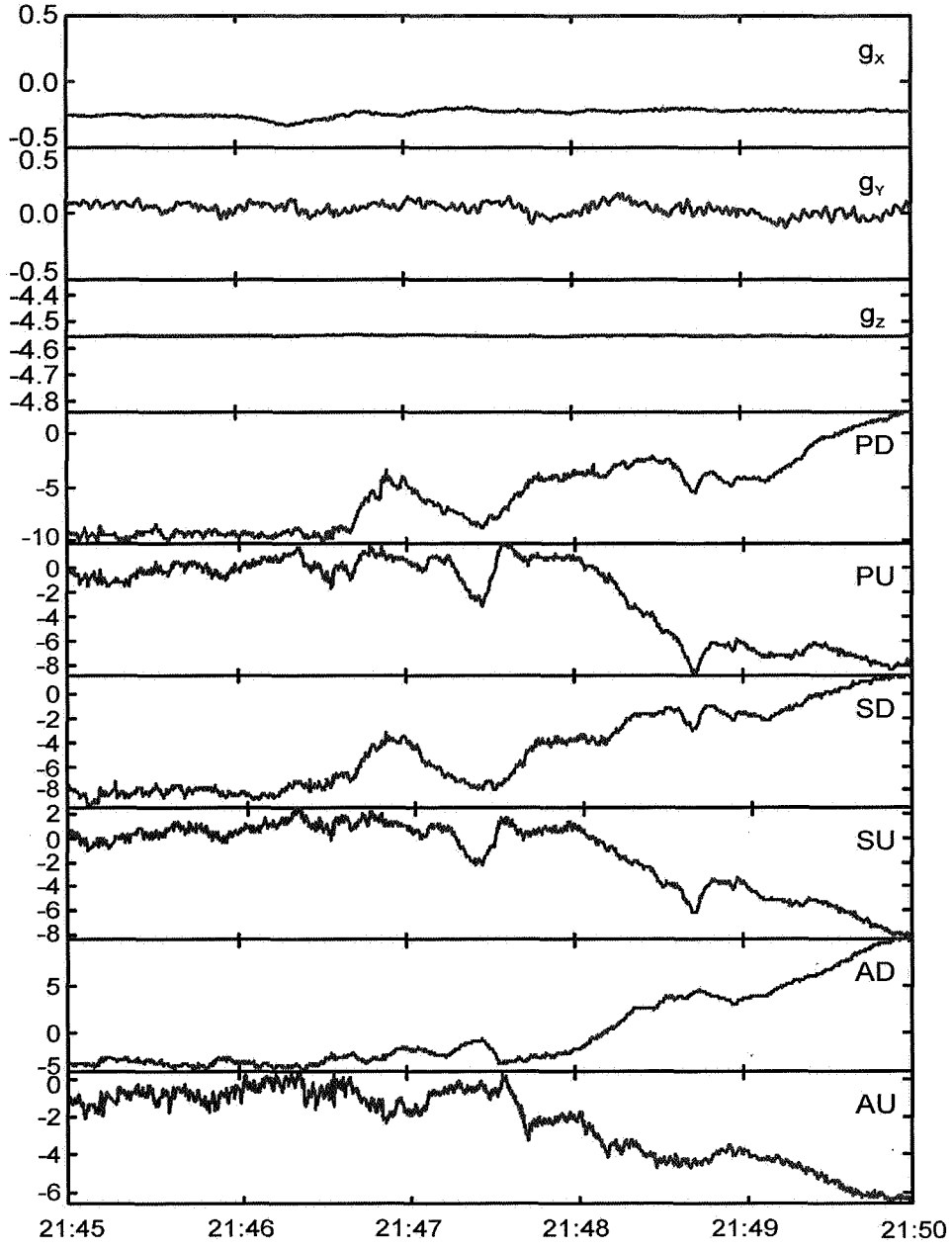

Figure 6. Ideal fields (top three plots) and mill outputs (bottom 6 plots) during a period when the Citation aircraft was not making calibration maneuvers. Note the features in the waveforms that are not due to roll and pitch changes. If we attempted to calibrate the aircraft mills using this section of data, the resultant $\mathbf{M}_P$ matrix would have almost nothing to do with the true matrix $\mathbf{M}$. Amplitudes are in V/m and the time scale is hours: minutes.

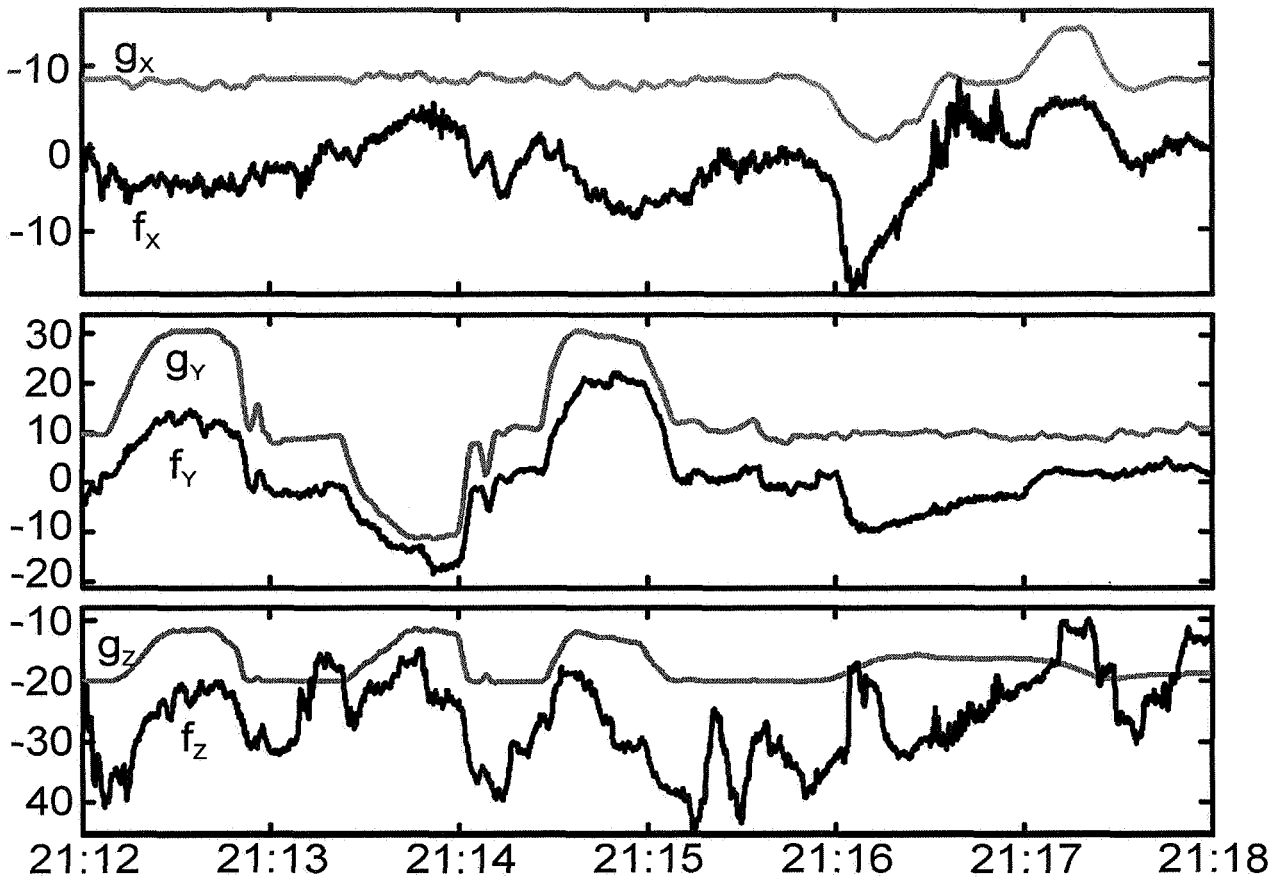

Figure 7. Ideal $(g_X(t), g_Y(t), g_Z(t), g_Q(t))$, gray waveform) vs. realistic $(f_X(t), f_Y(t), f_Z(t), f_Q(t))$, black waveform) fields during a flight of the North Dakota Citation. The amplitude is in V/m and the time is in hours: minutes on June 25, 2001. The black plots are the realistic fields based on the actual FM outputs while the gray plots are the ideal fields based only on the Gish field profile and the aircraft pitch and roll maneuvers (offset by 10 V/m to facilitate comparison).